Materials Advances

Accepted Manuscript

This article can be cited before page numbers have been issued, to do this please use: E. Guzman, G. Buell, S. Ruhunage, P. Müller, C. Risko and S. Thomas, *Mater. Adv.*, 2026, DOI: 10.1039/D6MA00553E.

ROYAL SOCIETY OF CHEMISTRY

rsc.li/materials-advances

View Article Online
DOI: 10.1039/D6MA00553E

ARTICLE

Impact of structure and connectivity of thiophene-based bicycles stacking with fluoroarenes in conjugated materials

Received 00th January 20xx,
Accepted 00th January 20xx

DOI: 10.1039/x0xx00000x

Elisa Guzman,[a] Gabrielle Buell,[a] Sashen Ruhunage,[b] Peter Müller,[c] Chad Risko,[b] and Samuel W. Thomas III*[d]

Noncovalent interactions between aromatic rings can dictate the crystal structures of organic optoelectronic materials. While cofacial interactions of fluorinated and non-fluorinated arenes are useful supramolecular synthons, the impacts of the structural details on these interactions remain unpredictable, particularly with the types of heterocycles common in materials derived from π-conjugated molecules. In this work, a combination of optical spectroscopy and X-ray crystallography demonstrates that both the degree of fluorination of a benzyl ester side chain and the regiochemical connectivity of a benzothiophene (BT) to an arylene-ethynylene backbone impact whether intramolecular cofacial stacking occurs or not. Surprisingly, the thienothiophene (TT) analog, which has an isoelectronic π-system with BT while a stronger electron donor when a part of donor-acceptor π-systems, did not show any evidence of cofacial stacking with fluoroarene side chains, regardless of the extent of fluorination. Quantum-chemical modelling rationalizes the dependence on BT regiochemistry, suggesting that while dispersion interactions comprise the largest individual component of attractive forces in stacking interactions, the strength of electrostatic interactions correlates best with the likelihood of intramolecular stacking interactions occurring in the solids. Finally, many of these molecules show polymorphic behaviour, with examples of blue-shifting and red-shifting mechanofluorochromism. Overall, this work enhances our ability to harness local structural details in deploying non-covalent interactions for designing solid state structures of optoelectronic materials.

Introduction

The molecular design of organic optoelectronics[1-5] must consider the π-conjugated backbone moieties[6-11] as well as the side chains,[12-15] for purposes of solubility and solid-state assembly[1, 16] to improve optoelectronic performance. Traditionally used for solubility,[17] the side chains[18-27] play a critical role in tailoring the materials properties and device performance.[28-33] Rational design using this approach, however, requires understanding of the noncovalent interactions that these functional side chains can introduce, particularly when involving the π-conjugated units of the main chain backbones of these materials.[34-36] While the Hunter-Sanders[37-39] and Wheeler-Houk[40, 41] models provide different explanations for the interactions between aromatic rings, each holds value in promoting rational design for noncovalent interactions for crystal engineering. [20, 26, 27, 34]

Considerations of noncovalent interactions amongst aromatic rings in organic optoelectronic materials is essential for materials design.[1-5] Our research group developed an arylene-ethynylene (AE) molecular scaffold to understand how molecular structural factors impact interactions of aromatic rings in solid-state assemblies;[42-49] the scaffold is derived from an AE with a central terephthalate flanked by aryl ethynyl groups.[44-46, 48] By including fluorinated benzyl benzoates on the central terephthalate, cofacial intramolecular interactions between the fluorinated side chain ring (ArF) and the conjugated flanking ring (ArH) can occur. For intramolecular cofacial interactions, the short benzyl ester tether requires the AE backbone to twist, interrupting what we would normally expect to be coplanar, maximally conjugated rings. When combined with intermolecular ArF-ArH cofacial interactions, this motif precludes aggregation between the chromophores, resulting in an optical gap for the material that resembles, or is hypsochromically shifted from, that of the molecule in dilute solution. We used this design to understand how structural characteristics in both the ArF and ArH rings, such as electronic substituent effects,[44-46, 50] electrostatic complementarity,[44, 47, 48] shape,[47, 49] and regiochemical effects[44, 46] correlate to whether cofacial "stacking" is observed in this scaffold and formation of polymorphs. We also demonstrated applications of these molecules through rational design of these interactions,

[a] Department of Chemistry, Tufts University, 62 Talbot Ave, Medford, MA, 01949, USA.
[b] Department of Chemistry & Center for Applied Energy Research (CAER), University of Kentucky, Lexington, KY, 40506, USA
[c] Department of Chemistry, Massachusetts Institute of Technology, Cambridge, MA 02139, USA.
[d] Department of Chemistry, University of Rochester, Rochester, NY 14627.
† Electronic supplementary information includes experimental procedures, NMR spectra, optical spectra, and crystallography information, See DOI: 10.1039/x0xx00000x

including phosphorescent solids and films that show reversible mechanofluorochromism (MFC) in both spectral directions.

Recently, we turned our attention to the noncovalent interactions of heteroaromatic ring systems.[48, 49] These investigations highlighted some correlations between both molecular shape and the mean electrical potential induced by a heterocyclic system at a typical π-stacking distance to whether ArF-ArH interactions of these rings occurs. Based on the importance of "local interactions" in the model of Wheeler and Houk[41], we were interested in the extent to which such variation might yield different results with heteroaromatic structures. In this work, we focus on the interactions of multiring fused thiophenes, which hold a privileged structural space in optoelectronic materials.[51-54]

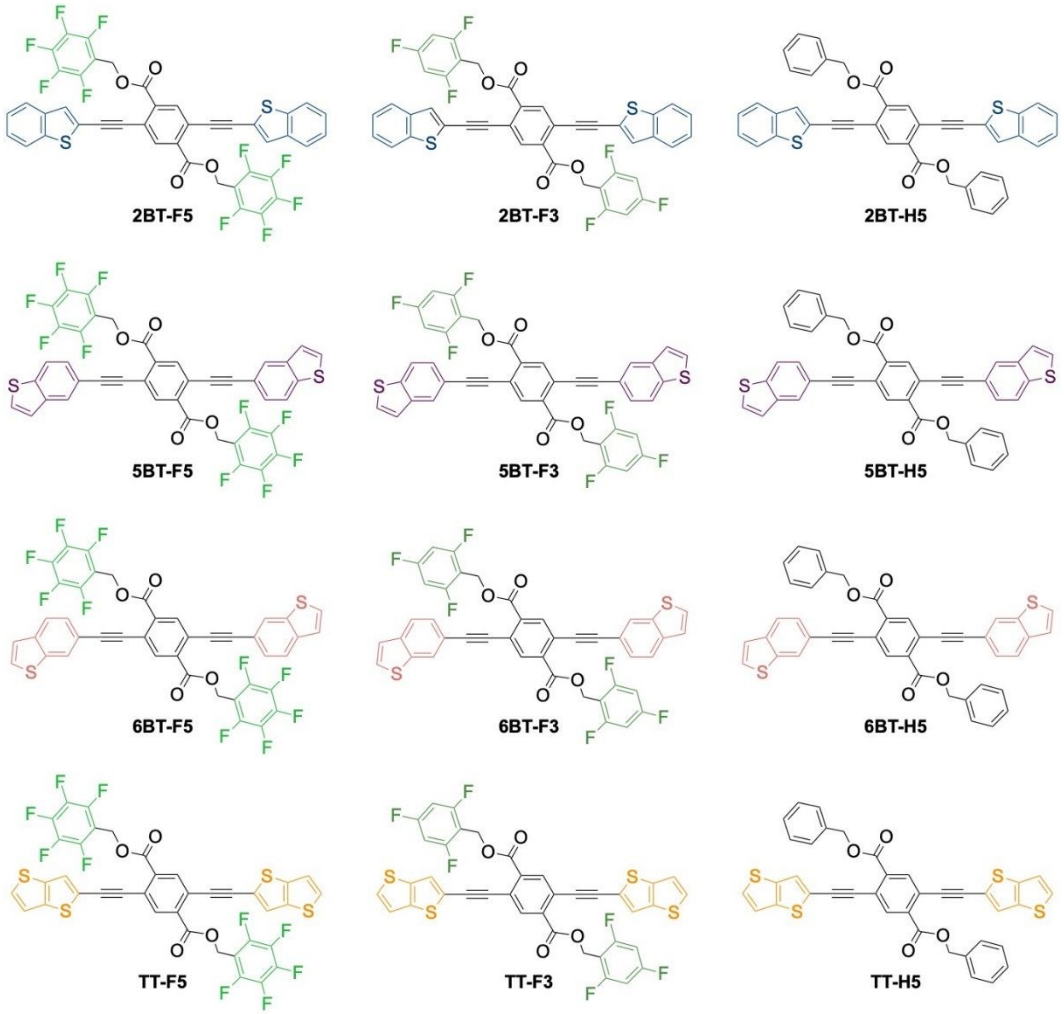

Chart 1. Structures of 12 molecules combining four conjugated heterocycles and three benzyl esters described in this study.

Results and Discussion

Experimental Design and Synthesis

Isomerism of conjugated backbones,[55] side chains,[56, 57] and even conformational isomers[58] can impact device performance. As an initial design to address the question of ArH regiochemistry, we chose the benzothiophene (BT) bicycle. BT is a common moiety in organic optoelectronics[53, 59, 60] , and one of the six heterocycles we studied previously in this AE scaffold. In our prior study, 2-benzothiophene showed both intermolecular and intramolecular coplanar ArF-ArH interactions and substantial bathochromic MFC of 67 nm (0.36 eV) in emission spectra. Of the six heterocycles we studied previously, this system has the most electropositive electrical potential computed at 3.25 Å, and its bicyclic structure enables stronger dispersion interactions than the smaller, monocyclic heterocycles thiophene and furan. We therefore attached the BT unit to our AE scaffold through either the 2, 5, or 6 positions. As a comparator, we also attached the thieno[2,3b]thiophene unit – in the 2 position – to the AE scaffold as another thiophene-based bicycle that is popular in organic optoelectronics, which we might expect to be more "electron rich" than benzothiophene, based on a typical descriptive parameter, i.e., yielding a molecule with higher energy HOMO (*vide infra*).

To test the regioisomerism impact on crystal structure, and therefore optical properties, we prepared each of these four conjugated backbones (**2BT**, **5BT**, **6BT**, and **2TT**) with one of three benzyl esters on the terephthalate: 2,3,4,5,6-pentafluorobenzyl (**F5**), 2,4,6-trifluorobenzyl (**F3**), and unfluorinated benzyl (**H5**). Our previous work indicated that reducing the number of fluorine atoms can tune the likelihood of observing ArF-ArH interactions, which we have ascribed to a combination of reduced electrostatic complementarity in the cofacial interaction and alternative interactions of the more electropositive C-H bonds in the **F3** ring.

These 12 target molecules were prepared using a straightforward strategy combining acylation of the appropriate benzyl alcohol with 2,5-dibromoterephthaic acid to yield the central unit, followed by combinations of Sonogashira and deprotection reactions to build the final targets. The precise nature of the Sonogashira reactions—which unit bore the terminal alkyne and which the halide—varied across the 12 molecules. Generally, the syntheses proceeded smoothly, with the exception of **5BT-F5**, the extreme insolubility of which frustrated our efforts to prepare, isolate and purify it. We attribute this in part to the strength of the ArF-ArH cofacial interactions (*vide infra*). By using 5-iodobenzothiophene together with 2,5-diethynylterephthalic acid, we were able to isolate a small amount of **5BT-F5** as a colorless solid; this lack of color was unusual, but important (*vide infra*), as all the other compounds isolated in this study were yellow in color, even after multiple recrystallization steps.

Optical Spectroscopy

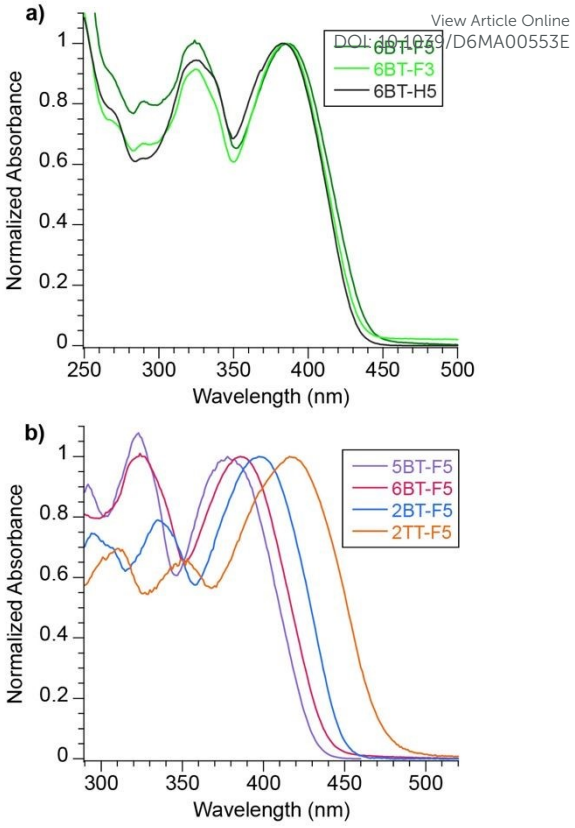

Figure 1. a) Absorbance spectra for 6BT-F5, F3, and H5. b) absorbance spectra for the F5 analogs of each conjugated arene

The UV/vis absorbance and fluorescence properties of all 12 molecules were recorded in chloroform and are summarized in **Table 1**. All compounds showed absorbance spectra in the expected regions of the electromagnetic spectrum—the near-UV and violet. The absorbance spectra of the **F5**, **F3**, and **H5** derivatives of the same conjugated backbone were nearly identical, differing only by 1-7 nm in λ_{max} of the lowest energy band (Figure 1a). While modest, a trend in UV/vis spectral position of the four conjugated backbones is consistent, with **5BT** (λ_{max} = 383-386 nm) having the highest energy absorbance spectra, followed by **6BT** (377-378 nm), **2BT** (391-398 nm) and finally **2TT** (413-416 nm); Figure 1b shows height-normalized spectra for the four **F5** derivatives. Together, these four classes span 0.3 eV in λ_{max} values.

Preliminarily, with the three **BT** regioisomers, we can assess the extent of electron delocalization through the UV/vis spectra, with **5BT** being the least delocalized, and **2BT** being the most. This correlates to the number of bonds between the more π-donating, polarizable sulfur atom and the electron-withdrawing alkyne unit, suggesting a stronger donor-acceptor effect between this unit when the terephthalate unit is further bonds away from the sulfur atom. The longer-wavelength absorbance spectra of the

TT compounds, with each **TT** unit having two sulfur atoms two or four bonds away from the ethynylterephthalate, suggests the most donor-acceptor character of this group.

All 12 compounds fluoresce in solution, with relative quantum yields of fluorescence between 0.18 and 0.52. Fluorescence lifetimes measured by time-correlated single photon counting range from 0.8 – 2.1 ns. Trends in the fluorescence spectra positions of these molecules in solution follow the same pattern as the UV/vis spectra, with **5BT** emitting the highest energy photons, and **2TT** emitting the lowest, spanning wavelengths of maximum intensity from 442 nm – 491 nm. Between compounds with the same conjugated backbone, differences in calculated radiative and non-radiative rates of relaxation are modest (no more than 2x difference), with the exception of **5BT-F5**, which shows a non-radiative rate of relaxation of 1.3 x 10^9 s^{-1}, 4-5x faster than **5BT-F3** and **5BT-H5**. Preliminarily, we attribute this to the same strong ArF-ArH cofacial interactions that impede solubility.

To examine the solution-based optical absorption properties in more detail, density functional theory (DFT) calculations and time-dependent DFT (TDDFT) calculations were carried out at the ωB97XD/6-31G(d') level of theory. The DFT calculations were performed to optimize the ground states (S_0) of all molecules in two conformations: one wherein there are intramolecular noncovalent interactions between the TT/BT units and the benzyl moiety (closed) and one wherein the benzyl moiety does not interact with the TT/BT units (open, *vide infra*). We note that in all cases the closed conformation is the most energetically stable (see SI). Further detailed analysis is provided *vide infra*.

The DFT-optimized S_0 geometries were then used for time-dependent DFT (TDDFT) calculations at the ωB97XD/6-31G(d') level of theory to evaluate the natures of the excited state transitions. The $S_0 \rightarrow S_1$ vertical transitions, which are predominantly HOMO → LUMO transitions localized on the AE backbone, are quite similar whether the system is in the closed or open conformations. We note that the $S_0 \rightarrow S_1$ vertical transitions for the open conformations are 0.2 – 0.5 eV red-shifted with respect to the closed conformations. The TDDFT results demonstrate similar trends with experiment, wherein **5BT** and **6BT** have the largest transition energies, followed by **2BT** and then **2TT**. Importantly, the open conformations present $S_0 \rightarrow S_1$ vertical transition energies that are closest to experiment, suggesting that the open conformation may be preferred in solution.

Solid-state luminescence

To improve understanding of how chemical structure impacts the solid-state properties of these materials, we collected their luminescence spectra as thin films drop cast from chloroform. The films were heated to 100 °C for 10 minutes after casting to mitigate impacts of deposition conditions. In the analysis below, we compare emission spectra of these samples with the same molecules in dilute solution to highlight the specific impacts of solid-state packing. Several key trends emerge from these analyses.

All "H5" showed large bathochromic shifts in the solid emission spectra relative to those in solution. Shifts in the emission spectra ranged from 47-71 nm, seen in Figure 2, which we attribute to aggregation and/or planarization of the AE chromophore as a solid. Our prior work on this general class of compounds has revealed a strong correlation between an aggregated and/or planarized packing arrangement and these spectral properties. The lack of fluorinated rings precludes favorable ArF-ArH cofacial interactions, which might otherwise mitigate interchromophore aggregation.

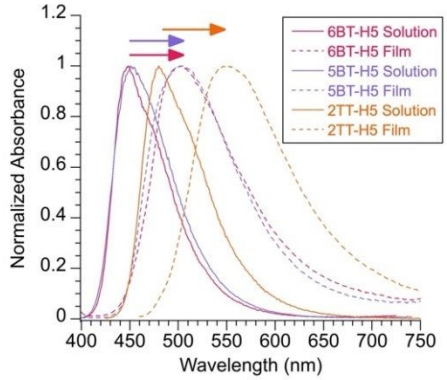

Figure 2. Bathochromic shifts of **H5** derivatives from solution to solid state.

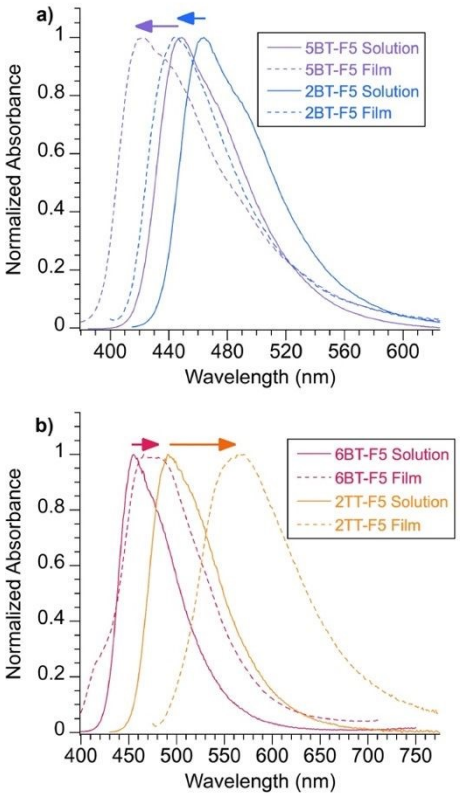

Figure 3. *a*. Hypsochromic shifts of emission spectra of **5BT-F5** and **2BT-F5** from solution to solid state. *b*. Bathochromic shifts of emission spectra of **6BT-F5** and **TT-F5** from solution to solid state.

In contrast, benzothiophene-F5 compounds showed hypsochromic or modest bathochromic shifts in their solid emission spectra relative to those in solution. Emission spectra of solids of **2BT-F5**, and especially **5BT-F5** are hypsochromically shifted from their emission spectra in dilute solution by 20 and 29 nm, respectively, (Figure 3) such that **5BT-F5** is a colorless solid that emits at an extraordinary blue wavelength of 422 nm, which is blue shifted from all the solution phase spectra reported here. Thin films of **6BT-F5** are only slightly bathochromically shifted from solution by 11 nm, suggesting a lack of strong J-aggregation compared to what is seen in **6BT-H5** (55 nm) and **6BT-F3** (55 nm).

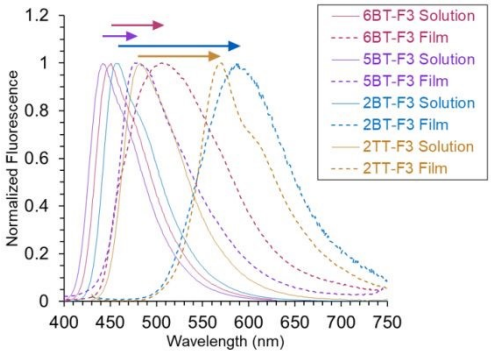

Table 1. Summary of the optical properties of the molecules from Chart 1.

	Solution (CH_2Cl_2)				Solid	
	λmax, abs (nm)	λmax, emis (nm)	Φ_F	τ (ns)	λmax, emis (nm)	Δλmax, emis (nm)
2TT-H5	416	480	0.32		551	71
2TT-F3	413	483	0.18	0.8	570	87
2TT-F5	416	491	0.18	0.9	567	76
2BT-H5[1]	391	443	nr	nr	529	86
2BT-F3	397	457	0.44	1.0	575	118
2BT-F5[1]	398	465	0.48	1.1	460	-5
5BT-H5	377	451	0.26	2.0	505	54
5BT-F3	377	442	0.52	2.1	477	35
5BT-F5	378	449	0.21	0.6	422	-27
6BT-H5	383	449	0.37	1.3	504	55
6BT-F3	384	451	0.31	1.3	506	55
6BT-F5	386	455	0.28	1.5	485	30

Figure 4. Emission spectra of the F3 molecules displaying a bathochromic shift of the solid state from the solution state

View Article Online
DOI: 10.1039/D6MA00553F

Curiously, and different from all the benzothiophene derivatives, emission of thin films of **TT-F5** show a bathochromic shift from solution phase spectra by 76 nm suggesting that these chromophores do aggregate, and likely do not participate in sufficiently substantial ArF-ArH stacking to prevent it. We initially found this result surprising, given its strong departure from **2BT-F5** and even the monocyclic thiophene in that position, which we reported previously. Finally, thin films of all four **F3** derivatives also showed large bathochromic shifts in their emission relative to solution state (Figure 5), similar to the **H5** derivatives, although the magnitude of shift for **5BT-F3** is slightly suppressed (35 nm) compared to the other three **F3** analogs (43-87 nm).

Polymorphism and Mechanofluorochromism

Table 2. Polymorphs observed of four compounds and summary of mechanofluorochromism (MFC) results.

	Emission Color	λmax, emis (nm)	MFC result
2TT-H5	Green	551	No
	Yellow	571	Yes, Green
2BT-F3	Green	501	No
	Yellow	588	Yes, Green
5BT-F3	Blue	456	Yes, Green
	Green	490	No
5BT-H5	Blue	495	Yes, Green
	Green	516	No

Since many of these solids have vibrant colors and show strong solid-state luminescence in the visible region of the spectrum, it can be relatively straightforward to observe polymorphs. In addition, mechanofluorochromism (MFC) is a common feature of this overall class of molecules, which also aids polymorph identification, and assists in understanding how different competing noncovalent interactions can derive formation of certain structures. While it is unlikely to be an exhaustive list, we have noted polymorph behavior without requiring mechanical grinding for four of the twelve molecules in this work (Table 2).

As the table indicates, many of these solids also display MFC, and the grinding-induced change of color can be either bathochromic or hypsochromic, depending on the molecule. In all examples here, however, MFC always favors more green emission, and moves the spectrum away from either blue or yellow/orange (see Figure S29). We attribute this observation to the fact that the conjugated backbones of these three molecules are all similar, with modest differences in spectra when in dilute solution (emission spectra within 50 nm). As demonstrated by powder X-ray diffraction experiments in prior work, mechanical grinding of this class of solids disrupts crystalline order, yielding amorphous solids. As described below, blue-shifted solids result from a crystalline order that requires ArF-ArH stacking and shielding of chromophores from aggregation, while strongly red-shifted solids result from J-aggregate arrangements of slip-stacked chromophores. In both cases, we conclude that grinding disrupts this crystalline order (either protection from aggregation or J-aggregation), yielding disordered solids with similar intermediate bandgaps, much like their similar solution-state emission spectra.

Single Crystal X-Ray Diffraction

We solved and refined six new single crystal X-ray structures. In general, the molecular structures found in the crystals conform to our expectations, as described above based on their optical spectra. Figure 5 shows four differing packing structures for the **5BT** backbone, depending on the side chains involved, while Figure 6 shows two other structures.

5BT-H5: Like most other "H5" derivatives of these types of chromophores, **5BT-H5** displays highly coplanar conjugated backbones with no more than 2° torsional angles. No substantial intramolecular noncovalent interactions are observable. The AE chromophores adopt slipped stacks with 3.4-3.5 Å interatom distances, and pitch and roll of 6 Å and 1.2 Å, respectively. Each phenyl side chain rings interacts in an edge-face manner on both faces, on one side with another side chain (2.8 Å H•••C distance) and on other side, with a hydrogen on the 6-position of the benzothiophene (2.7 Å H•••C distance). As a result of the interactions of the phenyl pendants, the slipped stacks of AE chromophores are not all along the same axes.

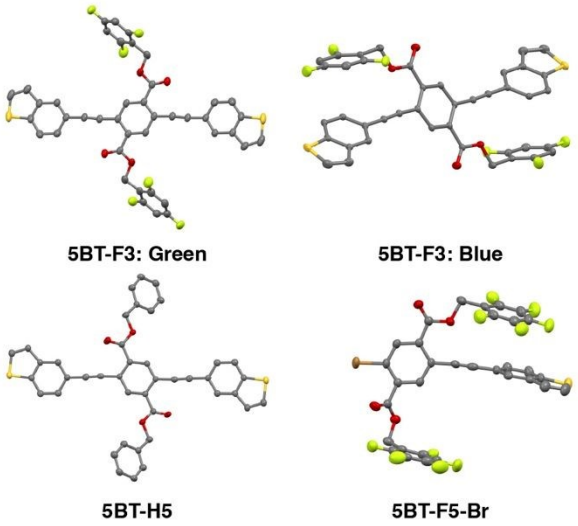

Figure 5. Four crystal structures of molecules in the **5BT** series showing a range of intramolecular torsional angles, depending on the range of side chain fluorinations. Thermal ellipsoids shown at 50% probability; hydrogen atoms removed for clarity.

5BT-F3: We were able to solve structures for both blue- and green-emissive polymorphs of **5BT-F3**. The blue-emitting polymorph shows ~40° twists between central and flanking rings along the AE backbone, with intramolecular interactions between the fluorinated and BT rings, that are cofacial but skewed, ~3.4 Å distances between 4 carbon of the F3 ring and carbons of the BT ring. Although there are also some intermolecular ArF-BT interactions (3.2 Å between F on F3 ring and fused BT carbon on another chromophore), obvious cofacial interactions between the chromophores (3.38 Å distance between BT carbons and carbons on terephthalate and alkyne) show evidence of aggregation.

The green-emitting polymorph of **5BT-F3** shows no obvious cofacial interactions of the fluorinated rings and clear signs of aggregation between highly coplanar AE chromophores. Approximately 3.5 Å separates some carbon atoms on parallel chromophores, and only 3.25 Å exists between the planes defined by the terephthalate

rings on adjacent chromophores. These chromophores adopt slipped stacks, with a roll of 2.5 Å and pitch of 3.7 Å.

5BT-F5-Br: Although the poor solubility of **5BT-F5** precluded us from growing X-ray quality single crystals, we were able to determine the structure of the "half" substituted arylbromide derivative **5BT-F5-Br**. This structure, seen in Figure 8, shows the characteristic twisting (~ 70° torsional angles) of the AE backbone and obvious intramolecular and intermolecular ArF-ArH cofacial interactions (close contacts of 3.3-3.4 Å), with the ArF ring bending towards the conjugated benzothiophene on the same molecule. The bromide appears to participate in a weak bifurcated halogen bonding arrangement with an alkoxy oxygen and fluorine atom. This overall arrangement, together with the insolubility of **5BT-F5** and that only **5BT-F3** shows any evidence of ArF-ArH interactions of the F3 derivatives suggests that the **5BT** regiochemical linkage has the most favorable interaction with the ArF rings of the ArH motifs described in this paper.

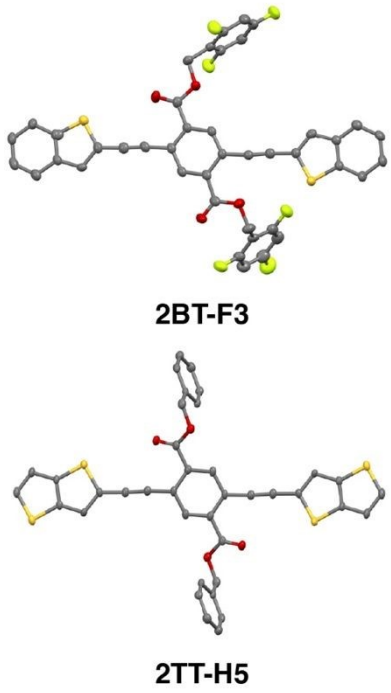

Figure 6. Single-crystal X-ray structures for coplanar AEs **2BT-F3** and **2TT**-H5. Thermal ellipsoids shown at 50% probability; hydrogen atoms removed for clarity.

2BT-F3: We previously reported a structure of **2BT-F5**;[48] it is twisted showing both intermolecular and intramolecular ArF-ArH interactions preventing cofacial interactions of the AE chromophores. In contrast, our new structure of **2BT-F3** (see Figure 6), which is yellow-orange in color**,** shows a coplanar AE backbone (torsional angles less than 5°) and a lack of ArF-ArH cofacial interactions. The AE chromophores are aggregated in two types of slipped co-facial arrangements and C-C contacts as short as 3.35 Å. A notable intermolecular C-H/pi interaction exists between an electropositive C-H on the F3 ring and a nearby aggregated chromophore.

2TT-H5: Like **5BT-H5**, **2TT-H5** shows highly coplanar AE chromophores (~4° torsions) with no notable intramolecular noncovalent interactions (Figure 6). The AE chromophores are arranged in slipped stacks (5.5 Å pitch, 1 Å roll), with 3.3-3.4 Å C-C distances as close contacts examples. The edge of phenyl side chains participate in edge-face interactions the with interior thiophene of the TT bicycle (2.9 Å C-S distance).

Intramolecular noncovalent interactions

To understand the molecular mechanisms by which these similar molecules choose a more twisted and "closed" conformation or a planar and "open" conformation, we turned to deeper analyses of the DFT optimized geometries (Figure 7; Tables S7-S10). Note that all closed and open conformations present no negative frequencies from normal mode analyses, suggesting that both conformations are minima on the potential energy surface. As noted above, the closed conformations are uniformly more stable than open conformations due to the additional dispersion and electrostatic interactions that close contacts bring. These calculations do not account for discrete interactions with solvent molecules that occur in solution, which would compete with the intramolecular interactions stabilizing the closed conformer. Moreover, for all four backbones, the F5 derivatives had the largest ΔE between closed and open conformations (Figure 8, ranging from 10 kcal/mol for **2TT** to 15 kcal/mol for **5BT**), suggesting the importance of electrostatic complementarity in these interactions. These results agree with our experimental observations, where in ranking the propensity for closed conformation in the perfluorinated derivatives is in the order **5BT**>**2BT**>**6BT**>>**2TT** based on the combination of crystallographic and fluorescence results, and suggest that the position of the sulfur atoms on the fused rings play a role in the preferred conformations.

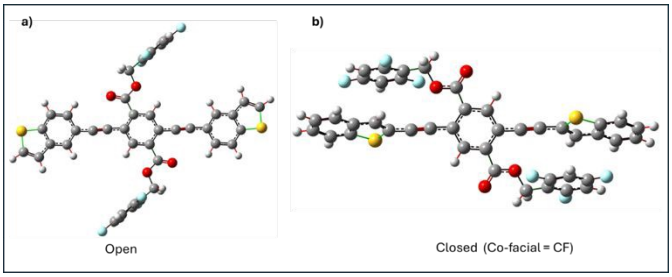

Figure 7. Geometries used in DFT computations. a) Depiction of open geometry, no twist in backbone, b) depiction of closed geometry where benzothiophene rings are twisted.

We used SAPT0/jun-cc-pVDZ (referred to as SAPT0) calculations to investigate the nature and strength of the intramolecular noncovalent interactions that may be responsible for these conformational preferences (Table S11). To focus on the interactions between aromatic rings, we examined only the interactions between unbound subunits of the molecules (ethynyl-substituted heterocycle and substituted benzyl ester) that were geometry-

optimized. Across the entire series, the total interaction energies fall across a small range, from –2.0 kcal/mol (attractive forces dominate) to +0.5 kcal/mol (repulsive forces dominate). Generally, those molecules with F3 or F5 pendants present stronger attractive binding energies when compared to H5. While trends within the decomposed contributions of the SAPT0 analysis are subtle, we note: i) the majority of the attractive energies in all cases are due to dispersion forces, and ii) the trend in the electrostatic components of the energies match the trend described above: **5BT**>**2BT**>**6BT**>**2TT** (Figure 8), again suggesting the electrostatic forces play an important role in selecting conformation in the crystal structure. We note that the molecular dipole moment of thienothiophene is zero, which may contribute to the smaller electrostatic contribution to noncovalent interactions.

Additionally, we carried out SAPT0 calculations on idealized systems where the stacking configurations were the same to account for structural variations in the optimized molecules. In these idealized structures, the distance between the BT/TT group and the aryl group was set 3.5 Å, the relative stacking configurations were the same, and the benzyl ester group was replaced with a benzyl hydroxyl group. In idealized cofacial systems, those with **5BT** present the smallest electrostatic interactions, suggesting that geometric relaxation from this idealized structure to that found in the optimized structure is crucial for maximizing the electrostatic interactions of the optimized state (Table S12-S13). We also examined idealized T-shape structures, keeping the same 3.5 Å interring distance, and looking at two configurations of the BT with respect to the aryl group (Table S14-S15). When the S atom on the BT is closest to the aryl moiety, the **5BT** molecules exhibit the largest attractive electrostatic interactions when compared to other systems, maintaining the **5BT** > **2BT** > **6BT** > **2TT** trend previously noted. When the S atom of the BT is pointed away from the aryl moiety, **6BT** systems exhibit strong electrostatic attractions, while those with **5BT** are smallest (or even most repulsive). These idealized structures reveal the importance of the stacking configurations found in the closed conformations on optimizing the noncovalent intramolecular interactions.

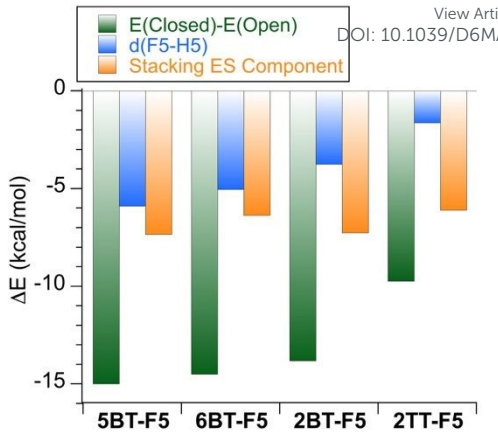

Figure 8. Comparisons of calculated energies of individual molecules containing the four different heteroaromatic backbones, including: i) the difference in energies between "closed" and "open" isomers, [*E(closed)* – *E(open)*], ii) the difference in [*E(closed)* – *E(open*)] comparing the F5 and H5 analogs in each backbone; in each case the F5 analog shows a larger preference for closed than the H5 analog, and iii) the electrostatic component of the F5-heterocycle stacking interaction of unbound subunits of the molecules (ethynyl-substituted heterocycle and substituted benzyl ester) that were geometry-optimized.

Conclusions

The optical properties of these twelve π-conjugated molecular solids deviate strongly from their behaviour in dilute solution, with impacts from both the identity and regiochemistry of the thiophene-based fused heterocycles, and the degree of fluorination of the benzyl ester side chains. The trends regarding electrostatic complementarity of the side chains align with our previous work, with heavily fluorinated side chains more likely to stack cofacially with the conjugated heterocycle, yielding hypsochromically shifted spectra of solids compared to their solution-state spectra. Among the four backbones, benzothiophene connected in the 5-position showed the most pronounced interactions, based on both the ~30 nm hypsochromic shift of solid-state luminescence compared to solution, and the insolubility of 5BT-F5. In contrast, the thienothiophene 2TT-F5 showed no evidence of intramolecular cofacial interactions, even while it showed the most donor-acceptor character in solution-phase optical spectra. DFT calculations rationalize these discrepancies, but only using crystallographically-informed geometries, instead of in idealized parallel cofacial stacks.

More broadly, these results advance rational design of noncovalent interactions of the ubiquitous thiophene-based fused heterocycles used in organic electronic materials. We find that differences in connectivity can influence in the solid-state optical properties in ways not apparent from experiments in dilute solution. Moreover, while models such as the polar-π framework are valuable for designing cofacial interactions broadly, our results emphasize that local structural details ultimate dictate solid-state arrangement. This is especially true when

comparing subtle changes to electrostatic landscapes, given that dispersion interactions comprise the largest fraction of attractive energy in the crystallographically realistic geometries calculated here. Finally, the MFC behavior of these molecules favors solution-like optical behavior upon grinding based on either disruption of J-aggregates (blue shifting) or twisted structures that lack aggregation (red shifting). These self-consistent trends inform rational design of force responsive fluorophores with predictable behavior.

Conflicts of interest

There are no conflicts to declare.

Data availability

Crystallographic data have been deposited at the CCDC with deposition numbers 2536219-2536224. Other data supporting this article (NMR spectra, optical spectra, and differential scanning calorimetry data) is available in the Electronic Supplementary Information.

Acknowledgements

Experimental work was supported by the National Science Foundation (NSF) under award DMR 2420040 and through the U.S. Department of Energy (DOE) Basic Energy Sciences (BES) through award DE-SC0016423. E.G. was supported by an NSF Graduate Research Fellowship. The work at the University of Kentucky (UK) was supported in part by DOE BES through award number DE-SC0016423 and the NSF through award DMR 2323422. S.R. and C.R. also acknowledge the UK Center for Computational Sciences and Information Technology Services Research Computing for their support and collaboration, and the use of Lipscomb Compute Cluster and associated research computing resources.

Notes and references

1. Yi, J.; Zhang, G.; Yu, H.; Yan, H., Advantages, challenges and molecular design of different material types used in organic solar cells. *Nat. Rev. Mater.* **2024,** *9* (1), 46-62.
2. Liu, C.; Xiao, C.; Xie, C.; Li, W., Flexible organic solar cells: Materials, large-area fabrication techniques and potential applications. *Nano Energy* **2021,** *89*, 106399.
3. Yan, C.; Barlow, S.; Wang, Z.; Yan, H.; Jen, A. K. Y.; Marder, S. R.; Zhan, X., Non-fullerene acceptors for organic solar cells. *Nat. Rev. Mater.* **2018,** *3* (3), 18003.
4. Lee, K.-W.; Wan, Y.; Huang, Z.; Zhao, Q.; Li, S.; Lee, C.-S., Organic Optoelectronic Materials: A Rising Star of Bioimaging and Phototherapy. *Adv. Mater.* **2024,** *36* (17), 2306492.
5. Riede, M.; Spoltore, D.; Leo, K., Organic Solar Cells—The Path to Commercial Success. *Adv. Energy Mater.* **2021,** *11* (1), 2002653.
6. Ding, L.; Yu, Z.-D.; Wang, X.-Y.; Yao, Z.-F.; Lu, Y.; Yang, C.-Y.; Wang, J.-Y.; Pei, J., Polymer Semiconductors: Synthesis, Processing, and Applications. *Chem. Rev.* **2023,** *123* (12), 7421-7497.
7. Lim, J. W., Polymer Materials for Optoelectronics and Energy Applications. *Materials* **2024,** *17* (15), 3698.
8. R. Murad, A.; Iraqi, A.; Aziz, S. B.; N. Abdullah, S.; Brza, M. A., Conducting Polymers for Optoelectronic Devices and Organic Solar Cells: A Review. *Polymers* **2020,** *12* (11), 2627.
9. Zhou, B.; Dai, T.; Zhou, J.; Chen, Y.; Geng, Y.; Lei, P.; Zheng, G.; Zeng, Q.; Zhou, E., Conjugated D–π–A photovoltaic polymers containing thieno[3,2-b]thiophene π-bridge. *Mater. Chem. Front.* **2024,** *8* (6), 1563-1590.
10. Kim, J.; Shirke, Y.; Milner, P. J., Flexible Backbone Effects on the Redox Properties of Perylenediimide-Based Polymers. *ACS Appl. Mater. Interfaces* **2024,** *16* (37), 48713-48721.
11. Xu, M.; Wei, C.; Zhang, Y.; Chen, J.; Li, H.; Zhang, J.; Sun, L.; Liu, B.; Lin, J.; Yu, M.; Xie, L.; Huang, W., Coplanar Conformational Structure of π-Conjugated Polymers for Optoelectronic Applications. *Adv. Mater.* **2024,** *36* (1), 2301671.
12. Lee, T.; Song, C. E.; Lee, S. K.; Shin, W. S.; Lim, E., Alkyl-Side-Chain Engineering of Nonfused Nonfullerene Acceptors with Simultaneously Improved Material Solubility and Device Performance for Organic Solar Cells. *ACS Omega* **2021,** *6* (7), 4562-4573.
13. Hu, A.; Nyayachavadi, A.; Weires, M.; Garg, G.; Wang, S.; Rondeau-Gagné, S., Unravelling the influence of side-chain symmetry on device performance: insights from isoindigo-based polymers in thin-film transistors. *RSC Appl. Polym.* **2023,** *1* (2), 292-303.
14. Yao, X.; Shao, W.; Xiang, X.; Xiao, W.-J.; Liang, L.; Zhao, F.-G.; Ling, J.; Lu, Z.; Li, J.; Li, W.-S., Side chain engineering on a small molecular semiconductor: Balance between solubility and performance by choosing proper positions for alkyl side chains. *Org. Electron.* **2018,** *61*, 56-64.
15. Biniek, L.; Fall, S.; Chochos, C. L.; Anokhin, D. V.; Ivanov, D. A.; Leclerc, N.; Lévêque, P.; Heiser, T., Impact of the Alkyl Side Chains on the Optoelectronic Properties of a Series of Photovoltaic Low-Band-Gap Copolymers. *Macromolecules* **2010,** *43* (23), 9779-9786.
16. Khasbaatar, A.; Xu, Z.; Lee, J.-H.; Campillo-Alvarado, G.; Hwang, C.; Onusaitis, B. N.; Diao, Y., From Solution to Thin Film: Molecular Assembly of π-Conjugated Systems and Impact on (Opto)electronic Properties. *Chem. Rev.* **2023,** *123* (13), 8395-8487.
17. Wang, C.; Ma, X.; Shen, Y.-f.; Deng, D.; Zhang, H.; Wang, T.; Zhang, J.; Li, J.; Wang, R.; Zhang, L.; Cheng, Q.; Zhang, Z.; Zhou, H.; Tian, C.; Wei, Z., Unique assembly of giant star-shaped trimer enables non-halogen solvent-fabricated, thermal stable, and efficient organic solar cells. *Joule* **2023,** *7* (10), 2386-2401.
18. Chochos, C. L.; Katsouras, A.; Drakopoulou, S.; Miskaki, C.; Krassas, M.; Tzourmpakis, P.; Kakavelakis, G.; Sprau, C.; Colsmann, A.; Squeo, B. M.; Gregoriou, V. G.; Kymakis, E.; Avgeropoulos, A., Effects of alkyl side chains positioning and presence of fused aromatic units in the backbone of low-bandgap diketopyrrolopyrrole copolymers on the optoelectronic properties of organic solar cells. *J. Polym. Sci., Part A: Polym. Chem.* **2018,** *56* (1), 138-146.
19. Çakal, D.; Demir Arabacı, E.; Yildirim, E.; Cihaner, A.; Önal, A. M., Side chain effect on the electrochemical and optical properties of thieno[3,4-c]pyrrole-4,6-dione based donor–acceptor donor type monomers and polymers. *Mol. Syst. Des.* **2023,** *8* (1), 65-78.

20. Cao, Z.; Li, Z.; Tolba, S. A.; Mason, G. T.; Xiong, M.; Ocheje, M. U.; Alesadi, A.; Do, C.; Hong, K.; Lei, T.; Rondeau-Gagné, S.; Xia, W.; Gu, X., Probing single-chain conformation and its impact on the optoelectronic properties of donor–accepter conjugated polymers. *J. Mater. Chem. A* **2023,** *11* (24), 12928-12940.
21. Tang, B.; Tang, S.; Qu, C.; Ye, K.; Zhang, Z.; Zhang, H., Side-Chain Engineering of Organic Crystals for Lasing Media with Tunable Flexibility. *CCS Chemistry* **2023,** *5* (10), 2348-2357.
22. Ma, D.-L.; Zhang, Q.-Q.; Li, C.-Z., Unsymmetrically Chlorinated Non-Fused Electron Acceptor Leads to High-Efficiency and Stable Organic Solar Cells. *Angew. Chem., Int. Ed.* **2023,** *62* (5), e202214931.
23. Gicevičius, M.; James, A. M.; Reicht, L.; McIntosh, N.; Greco, A.; Fijahi, L.; Devaux, F.; Mas-Torrent, M.; Cornil, J.; Geerts, Y. H.; Zojer, E.; Resel, R.; Sirringhaus, H., Impact of hydrophilic side chains on the thin film transistor performance of a benzothieno–benzothiophene derivative. *Mater. Adv.* **2024,** *5* (15), 6285-6294.
24. Holzer, I.; Lemaur, V.; Wang, M.; Wu, H.-Y.; Zhang, L.; Marcial-Hernandez, R.; Gilhooly-Finn, P.; Cavassin, P.; Hoyas, S.; Meli, D.; Wu, R.; Paulsen, B. D.; Strzalka, J.; Liscio, A.; Rivnay, J.; Sirringhaus, H.; Banerji, N.; Beljonne, D.; Fabiano, S.; Nielsen, C. B., Side chain engineering in indacenodithiophene-co-benzothiadiazole and its impact on mixed ionic–electronic transport properties. *J. Mater. Chem. C* **2024,** *12* (10), 3686-3697.
25. Yu, P.; Zhen, Y.; Dong, H.; Hu, W., Crystal Engineering of Organic Optoelectronic Materials. *Chem.* **2019,** *5* (11), 2814-2853.
26. Nandi, A. K., A Review on Self-Assembly Driven Optoelectronic Properties of Polythiophene-Peptide and Polythiophene-Polymer Conjugates. *Langmuir* **2024,** *40* (18), 9385-9405.
27. Ning, L.; Han, G.; Yi, Y., Conformational and aggregation properties of PffBT4T polymers: atomistic insight into the impact of alkyl-chain branching positions. *J. Mater. Chem. C* **2019,** *7* (45), 14198-14204.
28. Xin, J.; Li, W.; Zhang, Y.; Liang, Q.; Song, C.; Zhao, Y.; He, Z.; Liu, J.; Ma, W., A review of nonfullerene solar cells: Insight into the correlation among molecular structure, morphology, and device performance. *Battery Energy* **2023,** *2* (2), 20220040.
29. Chauhan, M.; Singh, R. S.; Singh, A. K., Aggregation induced strong photoluminescence at room temperature in large-area C8BTBT thin films. *Synth. Met.* **2024,** *306*, 117624.
30. Yao, Z.-F.; Wang, J.-Y.; Pei, J., Controlling morphology and microstructure of conjugated polymers via solution-state aggregation. *Prog. Polym. Sci.* **2023,** *136*, 101626.
31. Ding, G.; Chen, T.; Wang, M.; Xia, X.; He, C.; Zheng, X.; Li, Y.; Zhou, D.; Lu, X.; Zuo, L.; Xu, Z.; Chen, H., Solid Additive-Assisted Layer-by-Layer Processing for 19% Efficiency Binary Organic Solar Cells. *Nano-Micro Letters* **2023,** *15* (1), 92.
32. Wang, J.; Wang, Y.; Bi, P.; Chen, Z.; Qiao, J.; Li, J.; Wang, W.; Zheng, Z.; Zhang, S.; Hao, X.; Hou, J., Binary Organic Solar Cells with 19.2% Efficiency Enabled by Solid Additive. *Adv. Mater.* **2023,** *35* (25), 2301583.
33. Chen, Z.; Yao, H.; Wang, J.; Zhang, J.; Zhang, T.; Li, Z.; Qiao, J.; Xiu, S.; Hao, X.; Hou, J., Restrained energetic disorder for high-efficiency organic solar cells via a solid additive. *Energy Environ. Sci.* **2023,** *16* (6), 2637-2645.
34. Jackson, N. E.; Savoie, B. M.; Kohlstedt, K. L.; Olvera de la Cruz, M.; Schatz, G. C.; Chen, L. X.; Ratner, M. A., Controlling Conformations of Conjugated Polymers and Small Molecules: The Role of Nonbonding Interactions. *J. Am. Chem. Soc.* **2013,** *135* (28), 10475-10483.
35. Hu, Y.-C.; Chen, L.-M.; Lin, Z.-L.; Lee, J.-W.; Wei, W.-C.; Ko, T.-Y.; Lo, C.-Y.; Hung, W.-Y.; Wong, K.-T., Suppressing intermolecular interactions for enhancing the performance of exciplex-based OLEDs. *J. Chin. Chem. Soc.* **2022,** *69* (8), 1485-1494.
36. Schramm, B.; Gray, M.; Herbert, J. M., Substituent and Heteroatom Effects on π–π Interactions: Evidence That Parallel-Displaced π-Stacking is Not Driven by Quadrupolar Electrostatics. *J. Am. Chem. Soc.* **2025,** *147* (4), 3243-3260.
37. Hunter, C. A.; Sanders, J. K. M., The nature of π-π interactions. *J. Am. Chem. Soc.* **1990,** *112* (14), 5525-5534.
38. Cockroft, S. L.; Hunter, C. A.; Lawson, K. R.; Perkins, J.; Urch, C. J., Electrostatic Control of Aromatic Stacking Interactions. *J. Am. Chem. Soc.* **2005,** *127* (24), 8594-8595.
39. Cockroft, S. L.; Perkins, J.; Zonta, C.; Adams, H.; Spey, S. E.; Low, C. M. R.; Vinter, J. G.; Lawson, K. R.; Urch, C. J.; Hunter, C. A., Substituent effects on aromatic stacking interactions. *Org. Biomol. Chem.* **2007,** *5* (7), 1062-1080.
40. Wheeler, S. E.; Houk, K. N., Substituent Effects in the Benzene Dimer are Due to Direct Interactions of the Substituents with the Unsubstituted Benzene. *J. Am. Chem. Soc.* **2008,** *130* (33), 10854-10855.
41. Wheeler, S. E.; Houk, K. N., Through-Space Effects of Substituents Dominate Molecular Electrostatic Potentials of Substituted Arenes. *J. Chem. Theory Comput.* **2009,** *5* (9), 2301-2312.
42. Thomas, S. W.; Pawle, R. H.; Smith, Z. C., Stimuli-responsive side chains for new function from conjugated materials. *J. Photochem. Photobiol., A* **2016,** *322-323*, 119-128.
43. Thomas, R.; Varghese, S.; Kulkarni, G. U., The influence of crystal packing on the solid state fluorescence behavior of alkyloxy substituted phenyleneethynylenes. *J. Mater. Chem.* **2009,** *19* (25), 4401-4406.
44. Sharber, S. A.; Thomas, S. W., Side Chain Regioisomers that Dictate Optical Properties and Mechanofluorochromism through Crystal Packing. *Chem. Mater.* **2020,** *32* (13), 5785-5801.
45. Sharber, S. A.; Mann, A.; Shih, K.-C.; Mullin, W. J.; Nieh, M.-P.; Thomas, S. W., Directed Polymorphism and Mechanofluorochromism of Conjugated Materials through Weak Non-Covalent Control. *J. Mater. Chem. C* **2019,** *7* (27), 8316-8324.
46. Seth A. Sharber, Thomas, S. W., Small Changes With Big Consequences: Swapping Two Atoms In Side Chains Changes Phenylene-Ethynylene Packing And Fluorescence. *Chem. Eur. J.* **2018,** *24*, 16987-16991.
47. Mullin, W. J.; Pawle, R. H.; Sharber, S. A.; Müller, P.; Thomas, S. W., Programmed twisting of phenylene–ethynylene linkages from aromatic stacking interactions. *J. Mater. Chem. C* **2019,** *7* (5), 1198-1207.
48. Mullin, W. J.; Müller, P.; Schaefer, A. J.; Guzman, E.; Wheeler, S. E.; Thomas, S. W., Crystal engineering of heterocyclic arylene(ethynylene) oligomers through programmed aromatic stacking. *J. Mater. Chem. C* **2022,** *10* (31), 11199-11210.
49. Guzmán, E.; Yan, Y.; Müller, P.; Amengual, J.; Nieh, M.-P.; Thomas, S. W., Influence of shape on crystal structure and optical properties of heterocyclic conjugated molecules. *J. Mater. Chem. C* **2025**, *13*, 954-962.
50. Sharber, S. A.; Baral, R. N.; Frausto, F.; Haas, T. E.; Müller, P.; Thomas, S. W., Substituent Effects That Control Conjugated

View Article Online
DOI: 10.1039/D6MA00553E

Oligomer Conformation through Non-covalent Interactions. *J. Am. Chem. Soc.* **2017,** *139* (14), 5164-5174.
51. Shafiq, I.; Khalid, M.; Maria, G.; Raza, N.; Braga, A. A. C.; Bullo, S.; Khairy, M., Use of benzothiophene ring to improve the photovoltaic efficacy of cyanopyridinone-based organic chromophores: a DFT study. *RSC Adv.* **2024,** *14* (18), 12841-12852.
52. BiBi, S.; Kousar, Z.; Shafiq ur, R.; Bhatti, I. A.; Bhatti, H. N.; Khan, S. R.; Bai, F.-Q.; Farid, G., Newly efficient designed benzothiadiazole (A-D-A-D-A topology) based materials for organic photovoltaics: DFT Study. *Mater. Today Commun.* **2023,** *36*, 106481.
53. Pradeep Kumar, M.; Annie, A. S.; Kumar Bind, V.; Adithya, R.; Amaladass, P.; Dhayalan, V., A Review on Functionalization of Benzo-5,6-Fused Bicyclic Heteroaromatic Compounds. *Chem. Asian. J* **2024,** *19* (22), e202400455.
54. Usta, H.; Kim, D.; Ozdemir, R.; Zorlu, Y.; Kim, S.; Ruiz Delgado, M. C.; Harbuzaru, A.; Kim, S.; Demirel, G.; Hong, J.; Ha, Y.-G.; Cho, K.; Facchetti, A.; Kim, M.-G., High Electron Mobility in [1]Benzothieno[3,2-b][1]benzothiophene-Based Field-Effect Transistors: Toward n-Type BTBTs. *Chem. Mater.* **2019,** *31* (14), 5254-5263.
55. Chen, Z.; Zhu, J.; Yang, D.; Song, W.; Shi, J.; Ge, J.; Guo, Y.; Tong, X.; Chen, F.; Ge, Z., Isomerization strategy on a non-fullerene guest acceptor for stable organic solar cells with over 19% efficiency. *Energy Environ. Sci.* **2023,** *16* (7), 3119-3127.
56. Han, C.; Wang, J.; Zhang, S.; Chen, L.; Bi, F.; Wang, J.; Yang, C.; Wang, P.; Li, Y.; Bao, X., Over 19% Efficiency Organic Solar Cells by Regulating Multidimensional Intermolecular Interactions. *Adv. Mater.* **2023,** *35* (10), 2208986.
57. Fan, B.; Gao, W.; Zhang, R.; Kaminsky, W.; Lin, F. R.; Xia, X.; Fan, Q.; Li, Y.; An, Y.; Wu, Y.; Liu, M.; Lu, X.; Li, W. J.; Yip, H.-L.; Gao, F.; Jen, A. K. Y., Correlation of Local Isomerization Induced Lateral and Terminal Torsions with Performance and Stability of Organic Photovoltaics. *J. Am. Chem. Soc.* **2023,** *145* (10), 5909-5919.
58. Han, J.; Feng, J.; Kang, J.; Chen, J.-M.; Du, X.-Y.; Ding, S.-Y.; Liang, L.; Wang, W., Fast growth of single-crystal covalent organic frameworks for laboratory X-ray diffraction. *Science* **2024,** *383* (6686), 1014-1019.
59. Oza, N. H.; Kasundra, D.; Deshmukh, A. G.; Borane, N.; Boddula, R.; Patel, P. N., Benzothiophene based semi-bis-chalcone as a photo-luminescent chemosensor with real-time hydrazine sensing and DFT studies. *Environ. Sci.: Adv.* **2025,** *4* (2), 235-244.
60. Xie, P.; Liu, T.; Sun, J.; Yang, J., Structures, Properties, and Device Applications for [1]Benzothieno[3,2-b]Benzothiophene Derivatives. *Adv. Funct. Mater.* **2022,** *32* (21), 2200843.

View Article Online
DOI: 10.1039/D6MA00553E

Data Availability Statement:

Crystallographic data have been deposited at the CCDC with deposition numbers 2536219-2536224. Other data supporting this article (NMR spectra, optical spectra, and differential scanning calorimetry data) is available in the Electronic Supplementary Information.